ANL/XFD/CP-97663

Design and Performance of the 2-ID-B scanning x-ray microscope

I. McNulty, S.P. Frigo, C.C. Retsch, Y. Wang, Y.P. Feng, Y. Qian, E. Trakhtenberg, B. Tieman, B.-C. Cha, K. Goetze, and T. Mooney

Experimental Facilities Division
Advanced Photon Source, Argonne National Laboratory
Argonne, IL 60439

RECEIVED
SEP 28 1999
OSTI

W.S. Haddad

Lawrence Livermore National Laboratory, Livermore, CA. 94550 USA

The submitted manuscript has been created by the University of Chicago as Operator of Argonne National Laboratory ("Argonne") under Contract No. W-31-109-ENG-38 with the U.S. Department of Energy. The U.S. Government retains for itself, and others acting on its behalf, a paid-up, nonexclusive, irrevocable worldwide license in said article to reproduce, prepare derivative works, distribute copies to the public, and perform publicly and display publicly, by or on behalf of the Government.

*This work is supported by the U.S. Department of Energy, Basic Energy Sciences-Materials Sciences, under contract #W-31-109-ENG-38.

DISCLAIMER

This report was prepared as an account of work sponsored by an agency of the United States Government. Neither the United States Government nor any agency thereof, nor any of their employees, make any warranty, express or implied, or assumes any legal liability or responsibility for the accuracy, completeness, or usefulness of any information, apparatus, product, or process disclosed, or represents that its use would not infringe privately owned rights. Reference herein to any specific commercial product, process, or service by trade name, trademark, manufacturer, or otherwise does not necessarily constitute or imply its endorsement, recommendation, or favoring by the United States Government or any agency thereof. The views and opinions of authors expressed herein do not necessarily state or reflect those of the United States Government or any agency thereof.

DISCLAIMER

Portions of this document may be illegible in electronic image products. Images are produced from the best available original document.

SPIE Proc. 3449

Design and performance of the 2-ID-B scanning x-ray microscope

I. McNulty, S.P. Frigo, C.C. Retsch, Y. Wang, Y.P. Feng, Y. Qian,
E. Trakhtenberg, B. Tieman, B.-C. Cha, K. Goetze, and T. Mooney

Advanced Photon Source, Argonne National Laboratory, 9700 S. Cass Avenue, Argonne, IL 60439 USA

W.S. Haddad

Lawrence Livermore National Laboratory, Livermore, CA 94550 USA

ABSTRACT

We have constructed a high resolution scanning x-ray microscope at the 2-ID-B beamline at the Advanced Photon Source for 1-4 keV x-ray imaging and microspectroscopy experiments. The microscope uses a Fresnel zone plate to focus coherent x-ray undulator radiation to a 150 nm focal spot on a sample. The spectral flux in the focus is 10^8 ph/s/0.1% BW. X-ray photons transmitted by the sample are detected by an avalanche photodiode as the sample is scanned to form an absorption image. The sample stage has both coarse and fine translation axes for raster scanning and a rotation axis for microtomography experiments. The incident x-ray beam energy can also be scanned via the 2-ID-B monochromator while the sample is kept in focus to record spatially resolved absorption spectra. We have measured the performance of the instrument with various test objects. The microscope hardware, software, and performance are discussed in this paper.

Keywords: scanning x-ray microscope, microtomography, microspectroscopy, nanometer scale, 1-4 keV x-rays

1. INTRODUCTION

The 1-4 keV energy region is a rich but essentially untapped region for high resolution x-ray microscopy, microtomography, and microspectroscopy. The large number of K, L, and M electronic absorption features of elements in the middle of the periodic table, especially those with significant industrial and technological applications, provide strong motivation for development of an x-ray microscope with a spatial resolution in the 100-nm range and with three-dimensional and spectroscopic capabilities. For example, imaging of defects in buried multilevel aluminum structures in silicon based integrated circuits [1], and spatially resolved determination of sulfur speciation in contaminated catalysts [2] are attractive and feasible in this energy range.

Two-dimensional x-ray microscopy and micro-XANES between the carbon and oxygen K-edges (287 and 543 eV, respectively) at a resolution well below 100 nm has been under active development for some time [3-6]. Three-dimensional tomographic microscopy has been demonstrated at somewhat lower resolution using x-rays of these energies [7,8]. Recently, we proposed a design for a 1-4 keV scanning x-ray microscope (SXM) with the capability to record two-dimensional transmission scans, tomographic projections, and spatially resolved absorption spectra at the nanometer scale [9]. In this paper, we discuss details of the prototype instrument and its measured performance at the 2-ID-B undulator beamline at the Advanced Photon Source. The undulator source, beamline optics, monochromator, and experimental station are discussed elsewhere [10,11].

2. THE SCANNING X-RAY MICROSCOPE

2.1. Optics

The 2-ID-B scanning x-ray microscope is similar in design to the Stony Brook scanning transmission x-ray microscope at the National Synchrotron Light Source [12]. Fig. 1 is a photograph and fig. 2 is a schematic diagram of the instrument, which

operates in air. The 2-ID-B beamline delivers a partially coherent x-ray beam to the SXM through a silicon nitride exit window. A Fresnel zone plate (ZP) focuses the coherent portion of the beam to a diffraction-limited spot. A pinhole following the ZP acts as an order-sorting aperture (OSA) to select the first-order focal spot and exclude the other ZP diffraction orders, principally the zeroth. The sample is scanned through the ZP focus as the transmitted x-ray photons are detected with an avalanche photodiode (APD) and counted by a scaler. The sample stage, scaler, and other components of the SXM are controlled by a VME crate linked to a desktop computer workstation.

The ZP is made of 420-nm thick gold zones lithographically formed onto a 1-μm thick silicon nitride substrate. Its diameter is 77 μm and finest zone is 100 nm wide. When illuminated coherently, the ZP forms a transverse focal spot of size $\delta_t \approx 1.22\delta_r = 122$ nm (Rayleigh resolution criterion), where δ_r is the width of the finest zone. The longitudinal spot size (depth of field) is given by $\delta_l \approx 4.88\delta_r^2(E/hc)$, where E is the x-ray photon energy, h is Planck's constant, and c is the velocity of light. The first-order focal length of the ZP is approximately $f(E) \approx 2\delta_r R(E/hc)$, where R is the ZP radius.

The throughput of the SXM can be estimated from the diffraction efficiency of the ZP and the x-ray transmission of the system. At x-ray energies of 1-2 keV, the ZP behaves like a phase zone plate, i.e., the first-order diffraction efficiency is larger than the limiting value of $1/\pi^2$ for an amplitude zone plate with totally opaque zones. Fig. 3a shows the efficiency calculated using the theory of Kirz [13] and the Henke tables [14]. The ZP focal length limits the minimum air path through which the beam must travel. Consequently, the best-case air transmission is given by $T(E) = e^{-\mu(E)f(E)}$ where $\mu(E)$ is the mass attenuation coefficient for air. The ZP focal length (11.334 mm) is approximately equal to one absorption length (e^{-1}) in air at a photon energy of 1.825 keV. Fig. 3b shows the x-ray throughput of the ZP substrate and 250-nm thick beamline exit window, an air path equal to the ZP first-order focal length, and the product of these with the ZP diffraction efficiency.

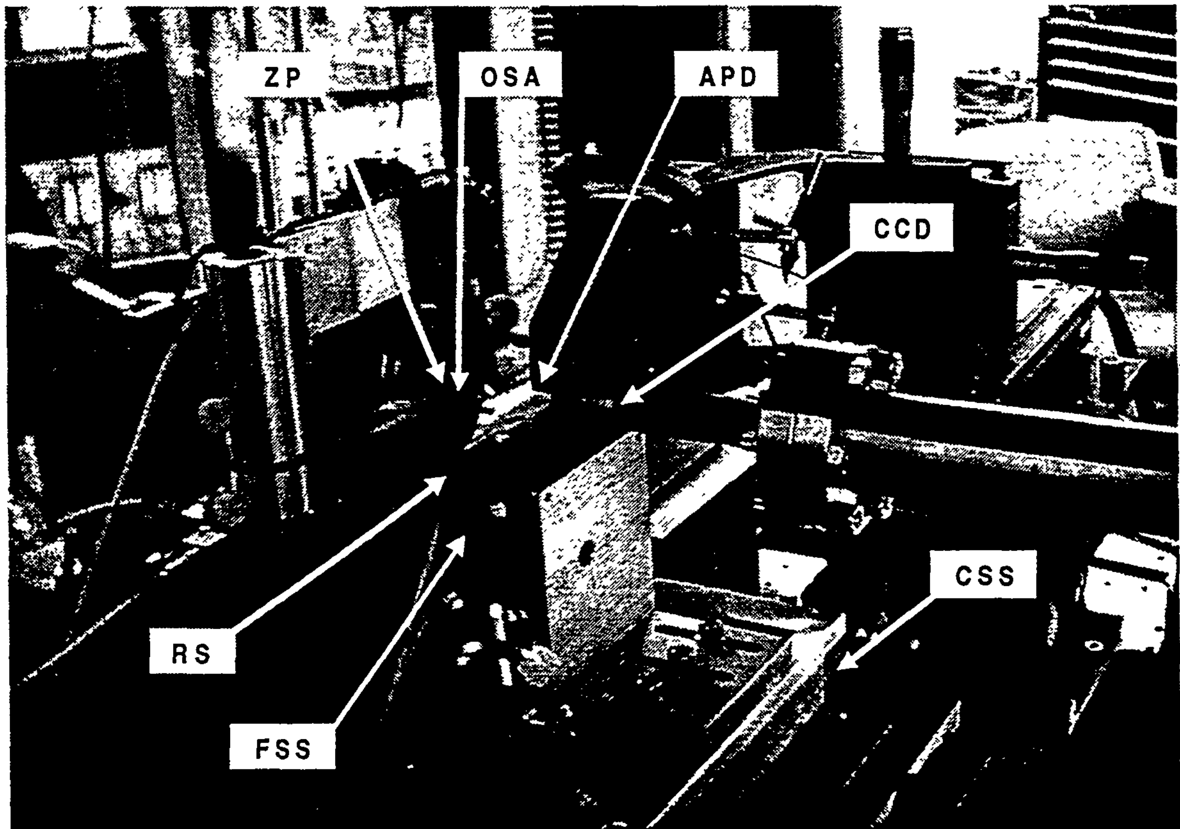

Fig. 1. Photograph of the 2-ID-B scanning x-ray microscope showing the major components: zone plate (ZP), order-sorting aperture (OSA), avalanche photodiode (APD), sample rotation stage (RS), fine scan stage (FSS), and coarse scan stage (CSS).

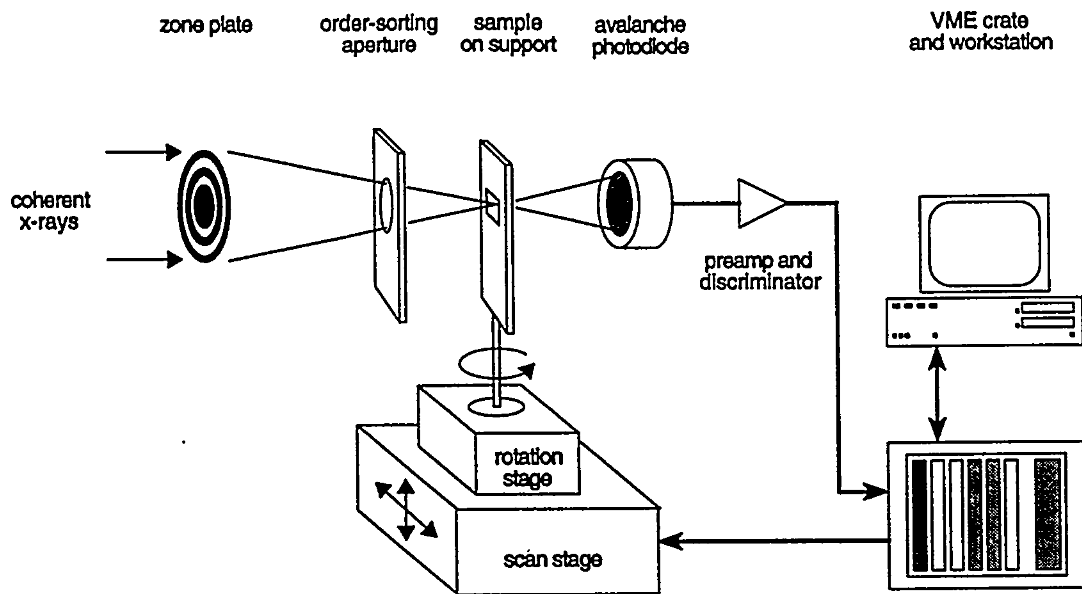

Fig. 2. Schematic diagram of the SXM.

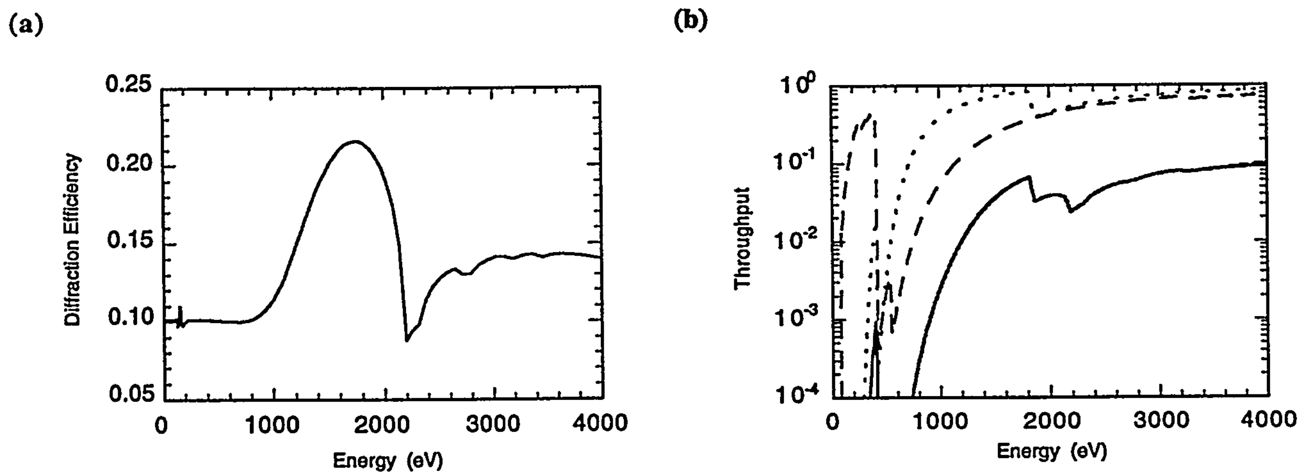

Fig. 3. (a) Calculated first-order diffraction efficiency of the ZP. (b) X-ray throughput of 1.25 μm of silicon nitride (dotted line), an air path equal to the ZP focal length (dashed line), and the SXM (solid line) including the silicon nitride, air path, and ZP efficiencies, as a function of x-ray energy.

2.2 Optics stages

The beamline exit window is supported on a manual four-axis positioning stage for alignment to the x-ray beam. Alignment of the ZP to the exit window is performed with a independent manual four-axis stage. Alignment of the OSA to

the ZP is performed remotely with a three-axis stage driven by picomotors (New Focus MRA-8351). The exit window, ZP, and OSA stage assemblies are supported together on a single linear stage oriented parallel to the beam (z axis), such that the ZP focus can be translated along the beam path without altering the relative alignment of these components to one another.

2.3 Sample stage

A useful feature of scanning microscopes is that they can be used to image a large or small field of view with the same microfocusing optics. This is accomplished in the SXM by using both fine and coarse resolution xy positioners to scan the sample. The sample stage assembly consists of a precision, low-mass, manual rotation stage, mounted on a fine scan stage, which is in turn mounted on a coarse scan stage. Samples are supported on an interchangeable pin held in a chuck on the shaft of the rotation stage, which was developed previously [7]. The fine scan stage (Queensgate Instruments S221-I) has two fast translation axes driven by electrostrictive actuators with a resolution of 6 nm and range of 100 μm. It employs integral capacitance micrometry for realtime position feedback and is directly controlled by a parallel digital interface (Xycom DIO XVME-240). The coarse stage (Newport M-UTM50PP.1 and New England Affiliated Technologies Z-Elevator) is driven by stepper motors and has a resolution of 0.5 μm, an x-axis range of 50 mm, and y-axis range of 15 mm. Custom software is used to control the scan stages, as described in the next section.

2.4 Control software

The control software used to operate the SXM is a three-component system based on EPICS (Experimental Physics and Industrial Control System), a toolkit for building distributed control systems [15]. The first component is a series of EPICS databases that runs under the VxWorks operating system on a 68040 processor board (Motorola MVME-532) in the VME crate. Process variables in this system are served to various client processes running in the VME processor, other processors, or remote workstations. This stand-alone computer contains all relevant process variables such as the scan stage position and the x-ray photon energy. High-level control routines required for scanning as well as low-level hardware interfaces are also present. The user can modify scan parameters both before and during scans as experimental conditions require. The core of the program is downloaded and launched automatically when the VME crate is turned on.

The second component is an X-compliant graphical user interface that runs as an EPICS client, in our case, under the Solaris (UNIX) operating system on the workstation (Sun Ultra 1 Creator/3D). Our user interface is written in IDL (Interactive Data Language, by Research Systems, Inc.), an array-oriented computational and graphical display package, and in MEDM (Motif Editor and Display Manager). The IDL interface plots one- and two-dimensional scan data as it is received from the VME crate. The two-dimensional display offers a variety of options, including a value-scaled color table representation of xy scans. All other control system variables are accessed via MEDM. It should be emphasized that the client application merely provides connections to the variables maintained by the VME-resident program through graphical objects (buttons, text entry fields, etc.). For example, the user interface displays all the SXM stage positions, detector values, the photon energy, and the beamline settings. Because the client maintains no state information, multiple copies of it can run simultaneously, serving local and remote experimenters in addition to technical support staff. Though normally controlled via the graphical user interface, the executable program can also be controlled by any other EPICS-compatible client including other VME-resident software. This allows the SXM to be coordinated with other EPICS-controlled hardware at run time.

The third control software component is a TCP/IP network connection between the VME crate and the client workstation, and a communications protocol called channel access. Channel access must be up and running on both the VME crate and the workstation for the SXM control software to function. This last component provides the glue which ties the other components together and enables integrated observation and control of the undulator, beamline, and SXM.

2.5 X-ray and visible light detectors

The APD detector assembly is mounted on a separate stage for independent alignment to the beam. In typical operation it is positioned just behind the sample to minimize absorption by air of the transmitted x-ray photons. The APD itself (EG&G Optoelectronics C30626F) is a silicon device with a 5 mm x 5 mm active detection area. It is operated near breakdown at a bias voltage of approximately 330 V. The pulse output corresponding to the detected x-ray flux is amplified (Phillips 6954-S100 preamplifier), discriminated (EG&G Ortec 935 constant-fraction discriminator) and counted (Joeger VSC-16 scaler) at each pixel in the scan. The APD is masked by a 1-mm-square 120-nm thick silicon nitride entrance window coated with 100

nm of aluminum to block ambient visible light. This coating attenuates visible light by roughly 10^6 yet only attenuates the x-ray beam by a few percent. The APD, which has not been optimized for peak performance, counts linearly up to 6 MHz and saturates at about 7 MHz due to pulse pileup in the readout electronics.

In addition to the APD we have integrated a large-format charge-coupled device (CCD) camera into the SXM for x-ray alignment, holographic and imaging microscopy experiments. The camera, adapted from a commercially available system (Princeton Instruments LN-CCD), uses a thinned, backside-illuminated, 1024 × 1024 pixel CCD array (SITe ST-003) with 24-μm square pixels. The CCD is liquid nitrogen cooled for low thermal dark current (~1 e^-/pixel/h) over long exposures. We modified the instrument by adding a 250-nm thick silicon nitride entrance window, vacuum beam transport tube, adjustable internal beam stop, and six-axis positioning stage assembly. As with the APD, the CCD entrance window is coated with 100 nm of aluminum. The beam transport tube is composed of standard conflat vacuum hardware which can be modified easily to meet a range of experimental requirements. Custom software written in C++ with an IDL display interface provides the necessary camera control, image acquisition, and display functions. The camera can also be controlled as an EPICS client via channel access, and may therefore be integrated with the SXM and beamline control software. The CCD camera is normally inserted downstream of the sample with the APD retracted from the x-ray beam.

Coarse alignment of the SXM components and sample is accomplished with a visible light microscope (VLM). The VLM consists of an interchangeable microscope objective (Edmund Scientific Plan 4x, 10x, or 40x) coupled to a monochrome video camera (Genesys GCB1324) on its own six-axis stage assembly. The optics and sample are illuminated from the side with a fiberoptic illuminator. The VLM also has a thin (<50 μm) phosphor screen that can be inserted into the focal plane of the objective lens to convert incident x-rays to visible light for detection by the video camera. We have found this real-time x-ray video system to be indispensable for rapid alignment of the SXM components to the x-ray beam following prealignment with visible light.

3. PERFORMANCE

3.1 Scan field linearity and orthogonality

The fine scan stage of the SXM demonstrates excellent reproducibility at the finest step size with which we have scanned it (35 nm). However, we observed that the angle between the x and y fine scan axes differs by approximately 14° from normal, and the dimensional scaling of both axes is off by about 40% from the true scaling. Fig. 4a shows a raw scanned image of a gold 1000-mesh grid (25.4-μm period). The apparent x and y scan ranges were about 70 μm in terms of the fine stage coordinates. The actual scan field is 103-μm square. However, simple rescaling of the x and y axes is made difficult by the nonorthogonality and curvature of the scan field, i.e., the x and y axes are not independent. Fig. 4b shows the same grid data after application of a first-order polynomial warping procedure to correct the image distortion and scaling correction using the known period of the grid. The coefficients of the polynomial used to warp the raw data were obtained by a least-squares fit of the raw data to a lattice of ideal grid points. Although there still remains a small degree of scan field curvature in fig. 4b, we are able to correct the principal distortion in scan data collected with the fine stage by this method. The same polynomial coefficients to correct the scan distortion can also be used to drive the fine scan stage directly in a properly scaled, orthogonal manner.

3.2 Imaging resolution

We measured the transverse imaging resolution of the SXM by a Foucault knife-edge test. For a well defined edge we used a 0.6-μm wide aluminum interconnect embedded in an ~10-μm thick SiO_2 matrix. This sample was fabricated and prepared by Digital Equipment Corp. as part of a study of electromigration defects in integrated circuits with the SXM [16,17]. By scanning over the interconnect with 71-nm steps and taking the derivative of the scan data, we determined the imaging resolution of the system to be 150 nm (fig. 5). The SXM thus operates near the diffraction limit of the ZP.

3.3 Focusing accuracy

A key consideration for microspectroscopy with the SXM is the accuracy with which the ZP focus can be targeted onto a specific feature of the sample while the photon energy is scanned. If the change in ZP focal length due to a change in photon

energy exceeds the ZP depth of field, the focusing stage trajectory must be straight enough so that the ZP can be refocused onto the sample without causing the focal spot to wander over it by more than the transverse spot size. We used the interconnect sample as a gauge to measure the ZP depth of field and the straightness of the focusing stage. The measured depth of field for this ZP is consistent with the expected value (e.g., 69 μm at 1.75 keV). The differential change in focal length with energy is 6.2 μm/eV. Therefore, energy changes greater than ~10 eV in the 1.5-2.0 keV range require refocusing of the ZP to the sample. We determined that the uncertainty in the transverse focus position at the sample at best focus due to focusing stage runout was about ±0.5 μm over energy scans of 50 eV in width.

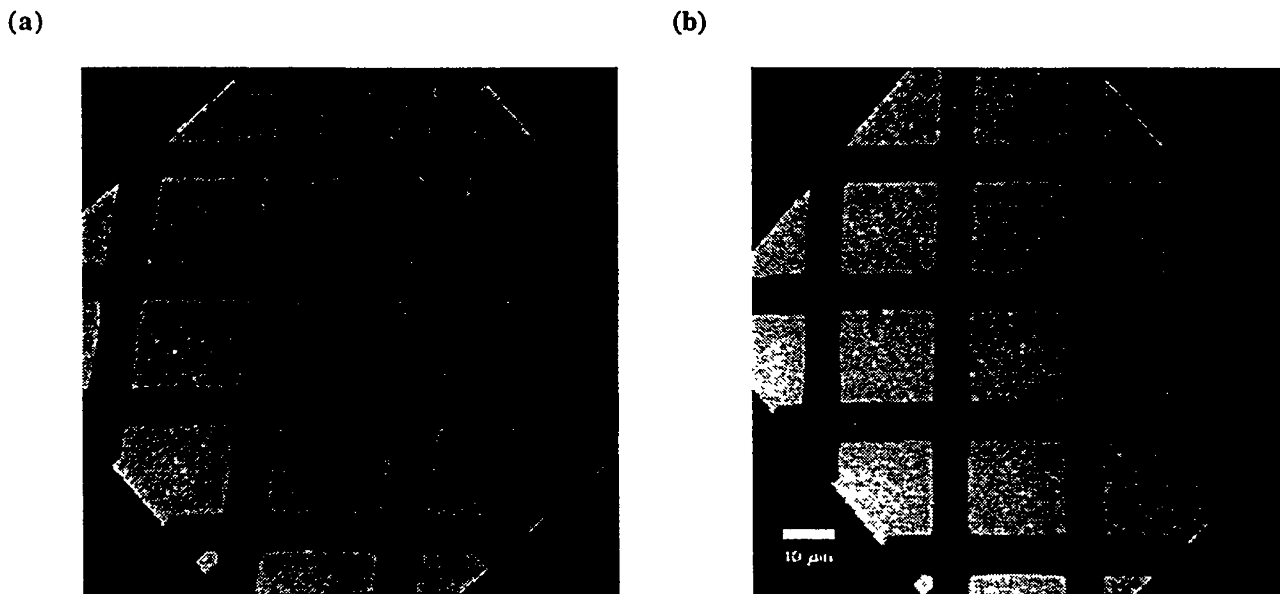

Fig. 4. (a) Raw scanned image of a 1000-mesh grid, after rotation to align the grid bars approximately along the horizontal axis. (b) Grid image after warping and rescaling. The actual length scale is shown.

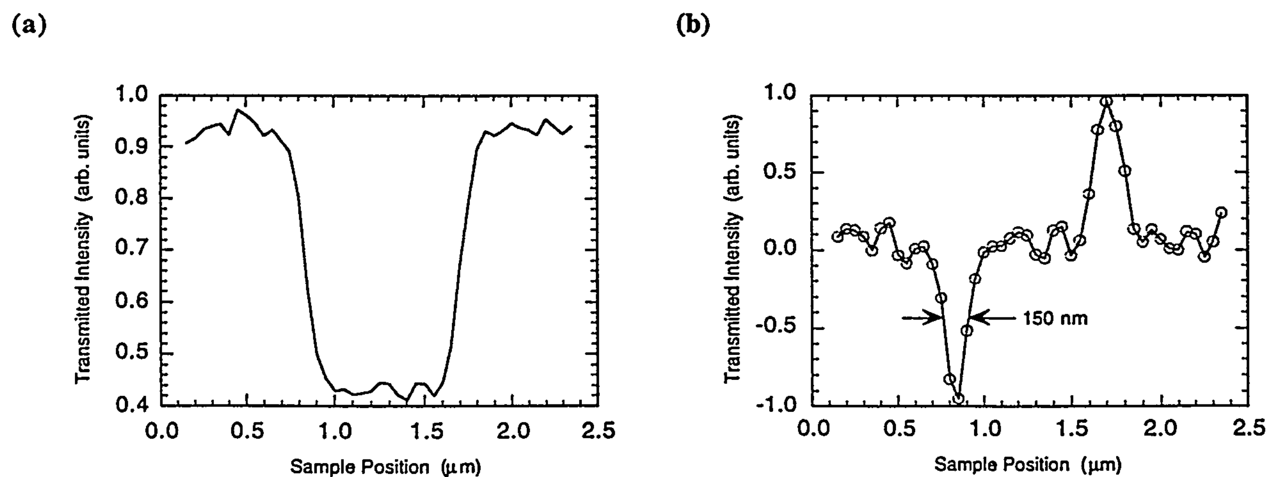

Fig. 5. (a) Knife-edge scan across an integrated circuit interconnect, and (b) its derivative, showing that the imaging resolution (focal spot size convolved with 71-nm scan steps and edge function of the interconnect) is about 150 nm.

3.4 Count rates and signal-to-noise ratio

The measured first-order ZP diffraction efficiency of 19% with 1.75-keV x-rays is close to the calculated efficiency. At this energy, we expect to obtain a spectral flux of 3×10^8 ph/s/0.1% in the ZP focus with an undulator source brilliance of 2×10^{18} ph/s/mm^2/mrad^2/0.1% BW [7], full-width at half-maximum source area of 0.05 mm^2 [7], beamline throughput of ~5% [11], ZP acceptance of 1×10^{-12} mrad^2, and SXM throughput of ~5%. Under typical operating conditions (100-µm beamline entrance and exit slit settings, 100 mA of current in the APS storage ring) and without a sample present in the SXM, the APD saturates at the ZP focus. By extrapolating from the count rate measured with the APD moved downstream by an additional 25 mm, we estimate that the focused flux is at least 10^8 ph/s/0.1% BW at 1.75 keV when the absorption due to the air path are taken into account.

In practice we observed that the time-averaged signal-to-noise ratio in this count rate is 0.1% at best due to 10-30 Hz instabilities in the source and beamline optics. This is an order of magnitude worse than that due to Poisson counting statistics alone. Nonetheless, the actual statistics at present are good enough to conduct worthwhile imaging experiments in many cases.

3.5 Scan speed and dead-time

The current VME hardware and EPICS software (version 3.13.2) we are using are capable of as little as 6 ms of software overhead or dead-time in tight scan loops that only involve moving the scan stage and reading the APD signal with the scaler at each scan pixel. The relatively high resonant frequency (>500 Hz) of the fine stage permits stage velocities exceeding 10 mm/s over its 100 µm range, or dwell times down to 10 µs for a 1000-pixel scan along the fast scan axis. On the other hand, with a focused spectral flux of 10^8 ph/s/0.1% BW we could afford to dwell for as short as 100 µs/pixel and still obtain 1% Poisson-limited photon statistics in each scan pixel. At these count rates the current software dead-time limits us to dwell times greater than a few milliseconds.

4. FUTURE DEVELOPMENTS

The SXM instrumentation is under active development in several areas. Most importantly, we plan to test zone plates with smaller finest zone widths. Many applications will clearly benefit by extending the resolution of the SXM below 100 nm. Also being developed is the capability to perform scans "on-the-fly" with the SXM, in which the timing of every pixel in each scan line will be handled entirely by the hardware in the VME crate. By contrast to the "step and repeat" scan method described above, the on-the-fly approach incurs a minuscule software overhead cost just at the start of each scan line rather than once for each pixel, thus enabling us to scan as fast as the scan stage assembly and photon flux permit. In order to record tomographic projections at finer angular resolution and without manual adjustment of the rotation axis, the sample rotation stage will be upgraded to a motorized system. To complement the standard transmission mode of operation we are implementing a solid state dispersive detector for scanning x-ray fluorescence microscopy experiments. This system, based on a low-energy Ge detector (Canberra GUL0035), is capable of measuring the fluorescence x-rays emitted by the sample, either in back-reflection mode or in transmission using thin samples. The energy resolution of the detector is 130 eV. Finally, for precise measurements along the beam path of the SXM we have built a white-light interferometric microscope with interchangeable objective lenses to replace the current VLM. This Michelson-type instrument will enable micrometer-scale sample and OSA prealignment while also providing a high resolution view of samples or components in the beam.

In addition to imaging test structures, we have begun to apply the 2-ID-B scanning x-ray microscope to various problems such as the study of integrated circuit defects. We anticipate that the range of problems that may be addressed with the SXM will increase in parallel to its capabilities.

5. ACKNOWLEDGMENTS

We are grateful to W. Yun and B. Lai for providing zone plate lenses, M. Kuhn for integrated circuit samples, Z. Levine and A. Kalukin for helpful suggestions concerning the design and user-friendliness of the instrument, and J. Arko for extensive help with its construction. This work is supported by the U.S. Department of Energy, Basic Energy Sciences, Office of Energy Research, under contract W-31-109-ENG-38.

6. REFERENCES

1. Y.C. Joo and C.V. Thompson, *J. Appl. Phys.* **81**, 6062 (1997).
2. A. Bensaddik, A. Caballero, D. Bazin, H. Dexpert, B. Didillon, and J. Lynch, *Appl. Catalysis* **A162**, 171 (1997).
3. H. Ade, X. Zhang, S. Cameron, C. Costello, J. Kirz, and S. Williams, *Science* **258**, 972 (1992).
4. G.D. Cody, R.E. Botto, H. Ade, S. Behal, M. Disko, and S. Wirick, *Energy & Fuels* **9**, 525 (1995).
5. C. MacGowan, et al., *Proc. Natl. Acad. Sci.* **94**, 6222 (1997).
6. G. Schneider, B. Niemann, P. Guttmann, and G. Schmahl, "Low-temperature x-ray microscopy of biological samples in amplitude and phase contrast," and C.J. Buckley and X. Zhang, "Characteristics and compensation of thickness effect in quantitative NEXAFS measurements," these proceedings.
7. W.S. Haddad, I. McNulty, J.E. Trebes, E.H. Anderson, R.A. Levesque, and L. Yang, *Science* **266**, 1213 (1994).
8. J. Lehr et al., *Optik* **104**, 166 (1997).
9. I. McNulty, Y.P. Feng, W.S. Haddad, and J.E. Trebes, *SPIE Proc.* **2516**, 217 (1995).
10. E. Gluskin, K.J. Randall, I. McNulty, W. Yun. A.M. Khounsary, and B. Lai, *J. X-ray Sci. Technol.* **5**, 29 (1995).
11. I. McNulty et al., *Rev. Sci. Instrum.* **67** (9), (1996) CD-ROM.
12. M. Feser, et al, "Applications and instrumentation advances with the Stony Brook Scanning Transmission X-ray Microscope," these preceedings.
13. J. Kirz, *J. Opt. Soc. Am.* **64**, 301 (1974).
14. E. Gullikson, et al., *Lawrence Berkeley Laboratory Report* **26259/UC-411** (1988).
15. L. Dalesio et al., "The Experimental Physics and Industrial Control System architecture: Past, present, and future," *Proc. 1993 Intl. Conf. on Accelerator and Large Experimental Control Systems* (Berlin, Germany), 18-22 October 1993; see also URL http://www.aps.anl.gov/asd/controls/epics/EpicsDocumentation/WWWPages/EpicsFrames.html.
16. Z.H. Levine, A.R. Kalukin, S.P. Frigo, I. McNulty, and M. Kuhn, "Tomographic Reconstruction of an Integrated Circuit Interconnect, " *Appl. Phys. Lett.*, in press.
17. A.R. Kalukin, Z.H. Levine, S.P. Frigo, I. McNulty, and M. Kuhn, "Effect of feature orientation in tomographic reconstructions," these proceedings.